Journal of Materials Chemistry C

Increased Crystallite Size in Thin Films of C60 and p-Terphenyls via PDMS-Assisted Crystallization

Journal:	*Journal of Materials Chemistry C*
Manuscript ID	TC-ART-09-2021-004516.R2
Article Type:	Paper
Date Submitted by the Author:	05-Feb-2022
Complete List of Authors:	Zhelyaskova, Vesta; University of Colorado Boulder, Electrical, Computer & Energy Engineering Sharma, Prachi; University of Colorado Boulder, Electrical, Computer & Energy Engineering Dron, Paul; University of Colorado Boulder, Department of Chemistry Martinez, Vikina; University of Colorado Boulder, Department of Physics Michl, Josef; University of Colorado at Boulder, Department of Chemistry Toney, Michael; University of Colorado at Boulder, Chemical and Biological Engineering; University of Colorado Boulder, Department of Materials Science and Engineering Dessau, Daniel; University of Colorado at Boulder, Department of Physics; University of Colorado Boulder, Renewable and Sustainable Energy Institute; University of Colorado Boulder, Center for Experiments on Quantum Materials Shaheen, Sean; University of Colorado Boulder, Electrical, Computer & Energy Engineering; University of Colorado Boulder, Department of Materials Science and Engineering; University of Colorado Boulder, Renewable and Sustainable Energy Institute; University of Colorado Boulder, Center for Experiments on Quantum Materials

ARTICLE

Increased Crystallite Size in Thin Films of C_{60} and *p*-Terphenyls via PDMS-Assisted Crystallization

SReceived 00th January 20xx,
Accepted 00th January 20xx

DOI: 10.1039/x0xx00000x

Vesta V. Zhelyaskova,*[a] Prachi Sharma,[a] Paul I. Dron,[b] Vikina Martinez,[c] Josef Michl,[b] Michael F. Toney,[de] Daniel S. Dessau[cfg] and Sean E. Shaheen[acefg]

Polydimethylsiloxane (PDMS)-assisted crystallization (PAC) is a scalable, solution-based method for growing crystalline organic semiconductor thin films, which can be used in a variety of electronic charge transport and device integration studies. Using this method, polycrystalline C_{60} and highly oriented crystalline *p*-terphenyl thin films can be grown out of solution onto amorphous substrates. Polarized optical microscopy, AFM, and GIWAXS characterization reveal that the films (1) are typically 100−200 nm thick, (2) are made up of needle- and tendril-like crystallites extending between 1−2.5 mm, and (3) have crystalline microstructures that vary with choice of solvent, temperature, and substrate pre-treatment. Both the small molecules are found to have some preferential growth parallel to the substrate. The *p*-terphenyl molecules arrange themselves end-on with respect to the substrate within the films—a potentially favorable orientation for in-plane charge transport. Films grown from carbon disulfide solutions cover larger areas more uniformly with thin needles compared with those grown out of *o*-dichlorobenzene. Growth at temperatures around ambient result in mm-long, uniformly aligned crystallites. Substrate pretreatment also enhances the uniformity and length of needle-like crystallites. This study's optimization of the PAC method parameters can promote accessible and scalable applications of crystalline organic small molecule thin films.

1. Introduction

Crystalline organic small molecules have several properties that make them attractive for high-throughput and large-scale electronic device applications. They can have carrier mobilities approaching those of polycrystalline silicon at room temperature ($\mu_p \sim 10^1$ cm^2 V^{-1} s^{-1} and $\mu_n \sim 10^0$ cm^2 V^{-1} s^{-1}),[1–4] well-defined electronic density of states,[5] and improved chemical and structural stability compared to amorphous organic materials.[6] Their electronic and chemical properties, however, are highly dependent on the morphology and degree of crystallinity of the material.[7–11] Thus, developing a versatile method for the controlled growth of crystalline organic small molecule thin films is essential for electronic device applications, especially at larger scales.

Small molecule organic thin films can be grown using many techniques including vapor deposition,[12] solvent evaporation-induced self-assembly,[13–15] and solvent exchange.[2,16,17] Growing organic active layers out of solution, however, has been shown to improve ordering and limit the formation of grain boundaries, thus enhancing charge mobility.[10,18–20] Solution growth of organic semiconductor thin films is especially attractive because the methods are usually inexpensive, easily scalable, and do not require extreme environments (i.e. high temperatures, low pressures).[21] In addition to the expanding breadth of organic materials that can be grown into crystalline thin films, several methods have been developed for crystalline orientation control (e.g. stamping,[2,22,23] capillary action,[19,23,24] controlled solution removal rate,[9,16,19,20] solution shearing,[25–27] surface pre-treatments[28,29]). The orientation, morphology, and degree of crystallinity of these films are often characterized using transmission electron microscopy, atomic force microscopy (AFM), and grazing incidence wide angle x-ray scattering (GIWAXS).

Overall, the most commonly solution-grown thin films are of the small molecule semiconductor 6,13-bis(triisopropylsilylethynyl) pentacene (TIPS-pentacene), C_{60}, and diketopyrrolopyrrole (DPP) for organic thin-film transistor and organic photovoltaic active layers.[14,30–33] Among the common solution growth techniques of meniscus-guided coating (MGC), spin-coating, and printing,[21] poly(dimethylsiloxane) (PDMS)-assisted crystallization (PAC) is a newer, less common method for organic thin film growth.[34] Solution growth methods using PDMS depend on (1) absorption of the solvent into the elastomer, (2) capillary action between the polymer and substrate, and/or (3) micron-scale physical templating. For example, PDMS can be pre-patterned as a stamp that can be used to localize the crystallization over desired areas, e.g. between electrical contacts.[23,35–37] The PDMS or a similar polymer, polyurethane acrylate, is often patterned with arrays of microchannels that facilitate the formation of crystalline nanowires by physically guiding the crystallization.[38–40] Furthermore, as a post-solution processing method, PDMS contact has been shown to encourage the growth of

[a] Department of Electrical, Computer and Energy Engineering, University of Colorado Boulder, 80309, USA.
[b] Department of Chemistry, University of Colorado Boulder, 80309, USA.
[c] Department of Physics, University of Colorado Boulder, 80309, USA.
[d] Department of Chemical and Biological Engineering, University of Colorado Boulder, 80309, USA.
[e] Department of Materials Science and Engineering, University of Colorado Boulder, 80309, USA.
[f] Renewable and Sustainable Energy Institute, University of Colorado Boulder, 80309, USA.
[g] Center for Experiments on Quantum Materials, University of Colorado Boulder, 80309, USA.

Electronic Supplementary Information (ESI) available: [details of any supplementary information available should be included here]. See DOI: 10.1039/x0xx00000x

much larger crystallites in already deposited amorphous thin films compared to those induced by thermal or vapor annealing.[22]

The PAC method explored in this study is similarly suited for the tailored growth of thin films of organic materials. This method, developed by Wu et al.,[34] uses *unpatterned*, cured PDMS to induce the crystallization of organic thin films from solution via the absorption of solvent. Films of rod-like small molecules with electronic properties grown using this PAC show higher degrees of orientation, which correlates to enhanced carrier mobilities.[41] The morphology and electrical properties of the films can further be optimized by varying growth parameters such as solvent, substrate, substrate pretreatment, and substrate temperature. Tuning the parameters to grow large crystallites with minimal grain boundaries and with well-oriented molecules enhances the lateral charge transport along the direction of π-π stacking.

Using the PAC method, we grew single-crystalline and polycrystalline thin films of C_{60}, *p*-terphenyl, and other organic small molecules out of *o*-dichlorobenzene (ODCB) and carbon disulfide (CS_2) solutions onto amorphous substrates. The PAC method first requires curing a slab of PDMS onto a glass slide and inverting it onto a clean substrate. A dilute solution of the organic material is pipetted between the substrate and the PDMS slab. As capillary action draws the solution towards the PDMS-substrate boundary, the PDMS absorbs the solvent. Now in a supersaturated solution, the small molecules easily precipitate out of solution and begin nucleating on the substrate. The crystal growth front moves away from the PDMS-substrate boundary leaving behind a crystalline thin film. A video of in-situ crystal growth can be found in the supporting files. Meniscus-guided coating via methods such as slot die coating, solution shearing, dip coating, and blade coating have been shown to induce similar long-range order in both polymers and organic small molecules as molecules crystallize onto the substrate out of the cast solution.[25,26] The same anisotropic shearing effect is likely introduced during PAC as the PDMS absorption of the solvent moves the supersaturated solution-substrate boundary away from the PDMS-substrate boundary.

The PAC method allows for controllable, anisotropic growth of organic crystalline thin films out of solution. Films can be grown out of a variety of solvents and onto either amorphous or crystalline substrates. Although large area, 100 µm-thick crystalline plates of *p*-terphenyl have already been grown out of solution,[42] using the PAC method we have grown 100 nm-thick *p*-terphenyl films with the longest crystalline needle-like domains reported to date. Using the same method, we grow needle-like crystalline thin films of C_{60} and other small molecule *p*-terphenyl analogues. C_{60} is a widely used organic semiconductor and *p*-terphenyl is an organic, rod-like molecule that has shown signs of a high temperature superconducting phase transition when doped.[43,44] With these two materials we explore the temperature dependence of and surface energy effects on organic crystal growth kinetics and estimate their respective crystal formation energies in the PAC system. This study's results elucidate the mechanisms behind this variation of PDMS-assisted crystallization and present pathways for further optimizing the crystal growth. Combining the versatility of the PAC method and our optimized parameters, many organic electronic materials beyond C_{60} and *p*-terphenyl can be cast into crystalline thin films with morphologies well suited for large-scale device integration.

2. Experimental Methods

2.1 Materials Synthesis

The *p*-terphenyl analogues were synthesized following typical Suzuki or Sonogashira coupling procedures and their NMR spectral characteristics are identical with those published.[45–50]

2.2 Sample Fabrication and Characterization

The PDMS slabs were prepared using the Dow Corning Sylgard 184 elastomer kit using a 10:1 base to curing agent ratio. The mixture was degassed, and a mass of 2.11 ± 0.05 g was drop-cast onto cleaned 3x1 inch glass slides. Slabs were cured on a hot plate at 100 °C for 3 hours. C_{60} (sublimed, 99.9%) was purchased from Sigma-Aldrich and used as received. The *p*-terphenyl and its analogues were synthesized as described above. Films were grown out of 50 µL of 1 mg/mL solutions of the organic small molecules prepared in CS_2 and ODCB. Films were grown on plain glass, glass with 50 nm thick evaporated gold contacts, and silicon wafers. Following sonication for 10 minutes in acetone, methanol, and isopropyl alcohol, substrates were further cleaned and prepared in an oxygen-plasma chamber. Substrates were pretreated with an octadecyltrichlorosilane (OTS) self-assembling monolayer (SAM). Cleaned substrates were soaked in a 5 mM solution of OTS in toluene for 12-15 hours. To terminate the SAM formation, substrates were rinsed and sonicated in toluene for 3 minutes, then dried with N_2 and immediately moved into an inert atmosphere for film growth. Substrates without the OTS pretreatment are referred to as "untreated." Samples prepared for GIWAXS analysis were grown on untreated silicon (to decrease noise) and annealed for 1 hour at 80 °C. Although the substrate is different, conclusions from analysis of films grown on untreated silicon (likely with a thin native oxide) can be cautiously extended to films grown on untreated glass.

Optical characterization was done using a Nikon Optiphot polarized optical microscope. AFM characterization was performed using the Asylum Research MFP-3D in tapping mode. GIWAXS data was collected using a beam of wavelength 1.54 Å under inert atmosphere. Data was collected using a Dectris EIGER 1M flat area detector and analyzed using the pyFAI and the pygix python libraries.

3. Results

3.1 Effects of Solvent and Substrate Pretreatment on Thin Film Growth and Crystallinity

The crystallinity of the films was first investigated using polarized optical microscopy (POM) and atomic force microscopy (AFM). C_{60} films grown out of ODCB showed long, angled crystallites as shown in Fig. 1a,b, with the growth direction pointed from the image top to bottom. The tendrils are polycrystalline regions of growth and the smaller crystallites of which they are comprised end in points with an average angle of 59.6° as indicated in Fig. 1a. Using optical density as a metric of thickness, the tendrils seem to grow thicker as the growth proceeds and more material is deposited on the substrate. This ODCB film growth is highly anisotropic and produces tendrils up to 2.5 mm in length, similar to those previously reported.[34] Although these polycrystalline fingers are long, they present large crack-like discontinuities, which would likely impede charge transport across them rendering them unsuitable for device active layers. Films grown out of CS_2 show similar anisotropic growth, but the crystallites are laterally much thinner, more needle-like, and more densely packed. Thin film growth from other solvents such as m-xylene have been

reported to result in the same needle-like growth for C_{60} crystallites.[14,34] POM reveals that the crystallites in the CS_2 films of both C_{60} and *p*-terphenyl are continuous and made up of more extensive single-crystalline domains (Fig. 1c–f). The occasional lateral cracks and grain boundaries as well as the periodicity of the needles are apparent in the AFM images and their line profiles (Fig. 2). These images show the microstructure of the films as an evaluation of the micron-scale charge transport pathways in the crystalline structures available for potential device integration. Furthermore, we extract the thickness of films grown out of CS_2 using AFM characterization. For C_{60}, film thickness ranged from 50 nm to 100 nm, while the *p*-terphenyl films were slightly thicker ranging from 100 to 150 nm—almost ten times thinner than those previously reported under similar growth conditions.[34] This difference can be attributed to the use of a twice as dilute solution in addition to an estimated 25% larger deposition area.

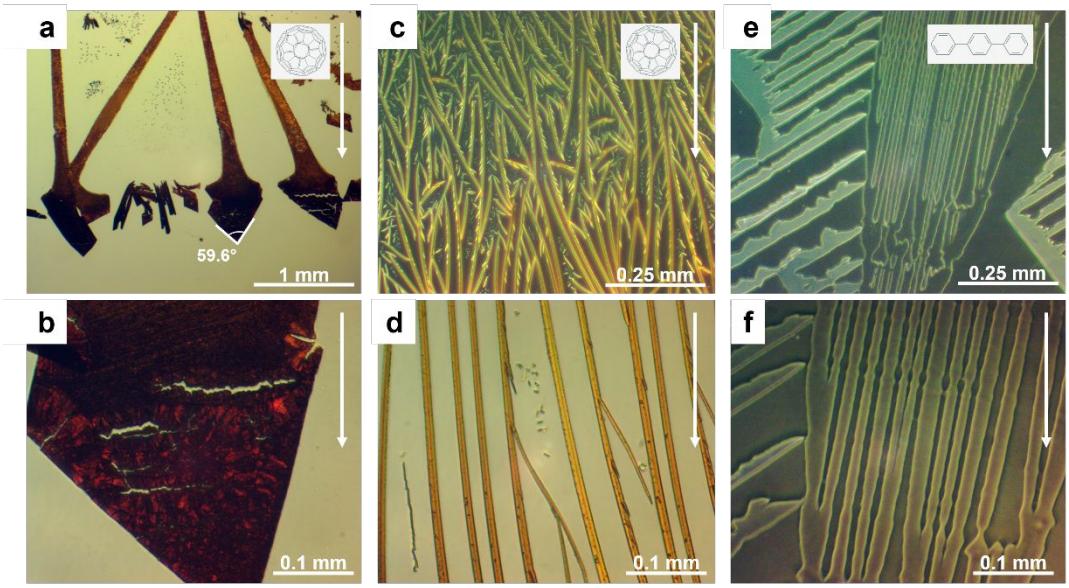

Fig. 1 POM images of two C_{60} thin films grown out of (a),(b) ODCB and (c),(d) CS_2 and (e),(f) a *p*-terphenyl film grown out of CS_2 using the PAC method. (b), (d), and (f) show the films of (a), (c), and (e) under 40x magnification. Direction of crystal growth is indicated by the arrow in each image. The chemical structures of C_{60} and *p*-terphenyl are shown in the subsets of (a),(b) and (c), respectively. Samples were all grown on SAM-treated glass substrates at room temperature. Cross polarizers were not orthogonally aligned in images (a), (b), and (d) to increase the visibility of the film.

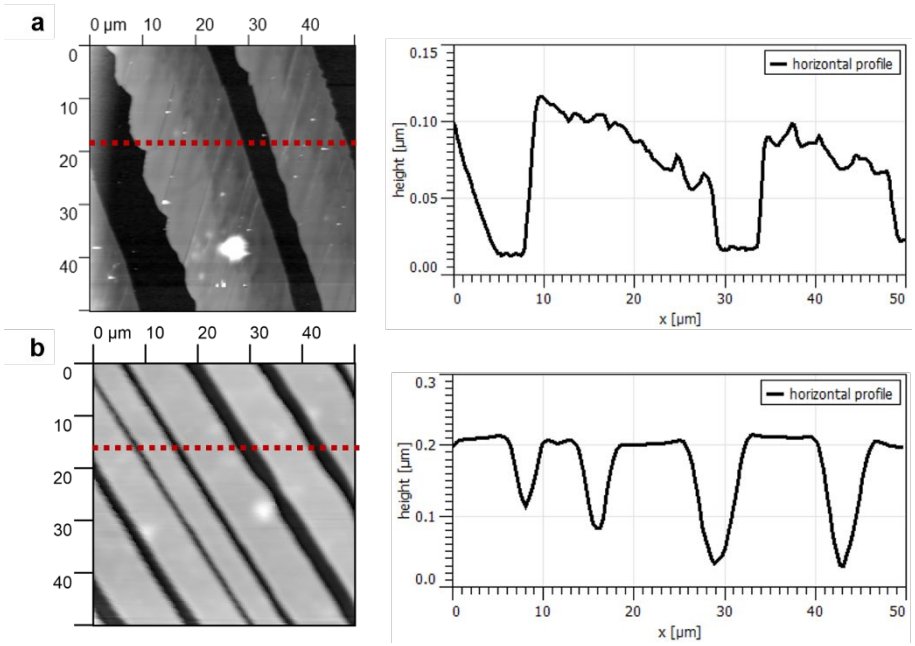

Fig. 2 AFM images and horizontal line profiles of (a) C_{60} and (b) *p*-terphenyl crystalline thin films grown using the PAC method out of a CS_2 solution on SAM-treated glass substrates at room temperature.

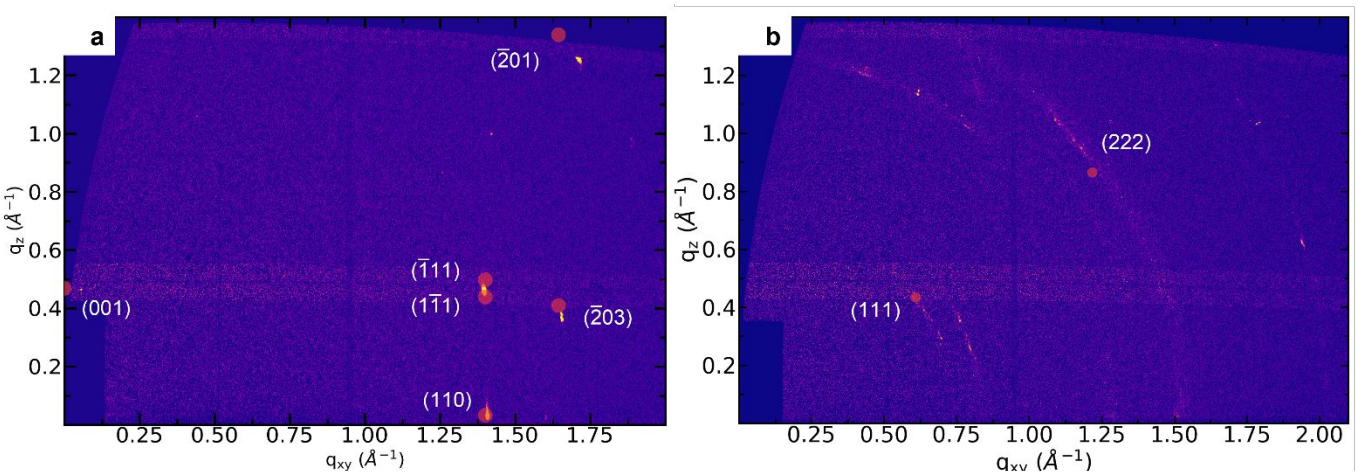

Fig. 3 GIWAXS diffraction patterns of (a) *p*-terphenyl and (b) C_{60} films grown using the PAC method. Both diffraction patterns indicate the crystallinity of the films, suggesting that the C_{60} film is a disordered combination of fcc and partially solvated crystal structures and the *p*-terphenyl film is composed of contracted monoclinic crystals. Calculated peak positions are indicated. Films were grown on untreated silicon substrates to reduce noise in the measurements.

Films of *p*-terphenyl analogues grown using the PAC method show similar anisotropic, needle-like growth in addition to variation in film morphology between different solvents (Fig. S1). Although the crystallinity of the *p*-terphenyl analogue thin films was not explored with XRD, POM imaging shows that molecular symmetry plays an important role in the molecules' ability to crystallize using the PAC method. Analogues with naphthalene cores could not crystallize out of either CS_2 or ODCB, whereas those with anthracene cores produced the needle-like growth characteristic of the *p*-terphenyl films.

The variety in crystallite morphology between different solvents can be attributed to the different molecule-solvent and solvent-PDMS interactions. Although the PAC method catalyzes crystal growth via the absorption and not evaporation of the solvent, the large difference in the polarity—and thus rate of uptake into the PDMS—of the solvents contributes to the difference in morphologies. The polarity of the solvent molecules tends to dictate how easily and quickly the hydrophobic PDMS can absorb the solvent to induce the supersaturated solution needed to spur nucleation. In experiments where PDMS was placed in solvents of different polarities, the solvent uptake—determined by the material's percent mass increase—was larger for nonpolar solvents compared to that for polar solvents. Table S1 summarizes these results. Thus, the faster uptake of nonpolar solvents will result in faster nucleation and crystallization. Furthermore, a small solvent-air boundary exists in the setup where the evaporation of the solvent may play a minor role in accelerating the supersaturation of the solution. Molecules in films grown from the less polar, more volatile solvents have significantly less time to diffuse and reorganize on the substrate. Both factors explain the lateral growth seen in films grown out of the more polar ODCB and the diminished lateral growth in crystallites grown out of the less polar, more volatile CS_2. A subtle change found in the color of the PDMS following the solution deposition suggests that the PDMS can also absorb some of the solute, which is expected to slow the rate of film growth by decreasing the concentration of the deposited solution. However, the magnitude of this effect on the final thin film growth is difficult to gauge in these experiments: the use of nonpolar solvent resulted in faster solvent uptake, but a change in material uptake was not quantified. Drop cast experiments show that the PDMS solvent uptake plays a significant role in reaching the supersaturation required to induce crystallization. ODCB solution cast on a treated glass slide takes more than twice the time (1 hour 45 minutes) to form a thin film than the same volume using the PAC method (45 minutes). The drop cast thin films have isotropic, spherulitic growth in contrast to the ordered, anisotropic films grown with PDMS (Fig. S2). In addition to solvent-PDMS interactions, molecule-solvent interactions exist within the C_{60} and *p*-terphenyl crystalline structures. In particular, the C_{60} lattice is likely solvated immediately after film growth, introducing solvent-induced crystal structures.[34,51,52]

Solute- and solvent-substrate interactions also affect the final quality of the crystalline thin films. Pretreatment of substrates with a SAM for organic thin film growth onto metals and oxides, especially pretreatment with OTS, is a common practice[53] and offers another avenue for optimization of PAC. In this study, glass substrates were pretreated with OTS to decrease the substrate's surface energy, improve surface uniformity, and reduce surface defect-induced trap states.[53,54] The change in surface energy was tracked using contact angle measurements. Fig. S3 shows the large increase in contact angle, or significant decrease in surface energy, after SAM treatment. Although crystalline thin films can still be grown on untreated amorphous substrates, the pretreatment promoted (1) the adhesion of the thin film to the substrate for both materials and (2) the growth of larger and more uniform crystallites for *p*-terphenyl (Fig. S4). Furthermore, C_{60} films grown out of ODCB on substrates without a SAM showed preferential nucleation and growth on the gold layer. With the addition of a SAM to the substrate there is no longer any preferential growth, and both the gold and glass have the same average nucleation density at the early stages of the film growth. However, surface activation using oxygen plasma prior to the deposition of the gold contacts and SAM will result in more uniform, preferential growth on the gold surfaces as described in the Supporting Information Section I. Following this procedure of surface hydroxylation and SAM pretreatment, PAC produces durable films

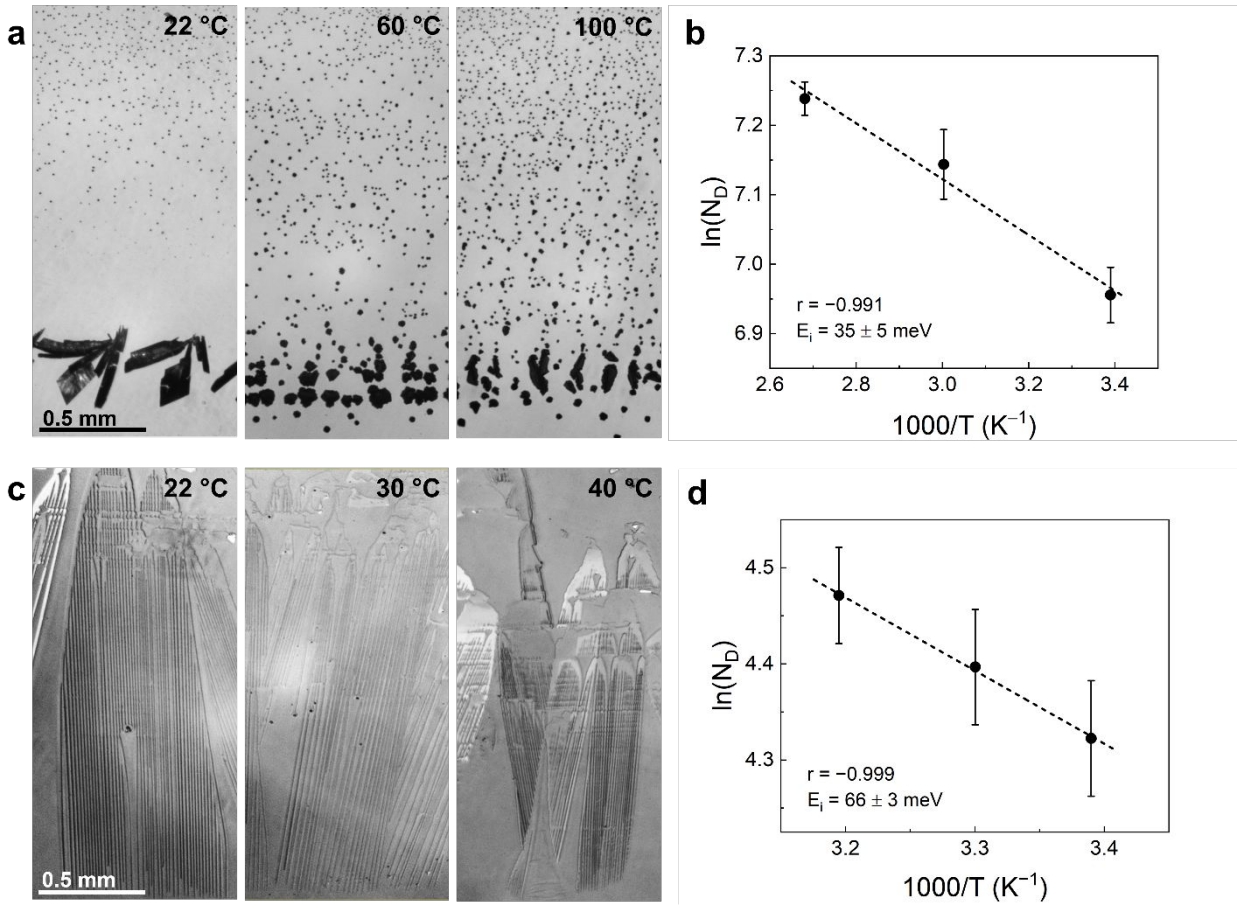

Fig. 4 Temperature dependence of crystal growth for (a),(b) C_{60} out of ODCB and (c),(d) *p*-terphenyl out of CS_2. Images in (c) have been contrast enhanced to improve visibility of crystalline needles. Plots of the change in nucleation density (surface and linear for C_{60} and *p*-terphenyl films respectively) with changes in substrate temperature show the expected Arrhenius dependence. E_i is the crystal formation energy calculated from the fit. Films were grown on SAM-treated glass substrates.

with large, uniform crystallites suitable for gold patterning and device integration.

GIWAXS characterization was performed to investigate the film structure and microstructure. GIWAXS data revealed the weakly oriented polycrystalline nature of the solution grown fullerene thin films. A mixture of the face centered cubic (fcc) (a = b = c = 14.78(5) Å) and partially solvated hexagonal-closed pack (hcp) or orthorhombic crystal phases are present in the C_{60} films.[51,55,56] This phase assignment agrees with the approximate 60° surface angles measured in the optical images (Fig. 1a), but it disagrees with results from the original PAC method study.[34] Because the C_{60} needle growth is anisotropic but with an orientational distribution, the 2D GIWAXS pattern consists of speckled arcs and rings (Fig. 3b). In contrast, the *p*-terphenyl films comprise of larger, more oriented crystalline domains of the monoclinic phase (a = 7.63(5) Å, b = 5.53(5) Å, c = 13.5(1) Å, α = γ = 90.0°, β = 92.0°) arranged in a herringbone fashion. The *p*-terphenyl 2D GIWAXS data (Fig. 3a) corroborate that from the POM; the sharp peaks confirm that the film is highly crystalline and very highly oriented with the (001) plane parallel to the substrate. Interestingly, the *p*-terphenyl x-ray diffraction reveals a contracted crystal structure relative to previously published data on the molecule's monoclinic crystalline phase.[57,58] The mismatch between the calculated and experimental peaks in the 2D data can be attributed to sample misalignment, as the integrated 1D data corroborates the indexing well. The indexed XRD data of both films are shown in Fig. S5. The χ−pole figure plots of the 2D GIWAXS intensity from both the C_{60} and *p*-terphenyl thin films can reveal the orientations of the crystallites' unit cells with respect to the substrate plane. The χ−pole plot of the C_{60} crystallites' (111) fcc planes (Fig. S6a) implies that the (001) plane, and thus the fcc unit cell, is preferentially oriented parallel to the substrate. The χ−pole plot of the *p*-terphenyl crystallites' ($11\bar{1}$) planes (Fig. S6b) reveals that the unit cells are also preferentially oriented nearly parallel to the substrate. Since the (001) plane is parallel to the substrate plane, the individual *p*-terphenyl molecules are oriented end-on on the substrate (Fig. S7). Edge-on or end-on orientation may be most desirable for device integration where the film lies between two contacts in plane with the substrate. Although it is dependent on the angle between adjacent molecules, the π-π stacking is likely to be largest in-plane with the molecules in an end-on arrangement, which orients the stacking in a potentially desirable direction for charge transport within the film.[7]

3.2 Effects of Substrate Temperature on Thin Film Growth and Nucleation Density

To investigate the effects of temperature on the kinetics of PAC, six C_{60} films were grown out of ODCB in an inert environment at substrate temperatures (T_S) of −20, 5, 22, 40, 60, and 100 °C. At low T_S, the crystallite growth is in a diffusion-limited regime. Increasing T_S up to the ambient (T_A = 22 °C) in this regime increases the diffusion rate allowing for the growth of larger, more uniform crystallites. As the temperature increases beyond T_A, the deposition rate increases, and the growth enters a desorption-limited regime. The latter growth regime was investigated by studying the impact of temperature on needle length and nucleation density. As described by Virkar et al.,[54] the nucleation density of the films is exponentially dependent on the inverse of the temperature as

$$N_D = R^{\alpha}\exp\left(\frac{-E_{des}+E_{diff}+\Delta G^*}{kT_S}\right) \quad (1)$$

where R is the deposition rate, α is a constant, E_{des} is the energy barrier to desorption, E_{diff} is the energy barrier to diffusion, and ΔG^* is the thermodynamic barrier to nucleation including surface energy effects. The sum $E_{diff} - E_{des} + \Delta G^*$ is the total energetic barrier to nucleation, E_i, and it can be related to the cohesive energy of the bulk material.[59] Since the barrier to desorption must be larger than the sum of the nucleation barrier and diffusion barrier for a film to form, the nucleation density is predicted to increase with increasing substrate temperature. Furthermore, increased solvent uptake by the PDMS cannot be ignored at higher temperatures as it likely increases the deposition rate, R. With accelerated deposition rates at temperatures greater than T_A, we expect the increased nucleation density to result in smaller crystallites.[54] However, the nucleation density's exponential dependence on E_i, implies that it is more affected by surface energy effects than by deposition rate (solvent evaporation, solvent uptake, etc.).

At the temperatures below T_A the C_{60}/ODCB thin films are comprised of smaller, feathered crystallites, a signature morphology for diffusion-limited organic crystal growth.[60] As T_S was increased to T_A the fractal patterns diminished, and the average crystallite size increased. As T_S was increased beyond T_A, the nucleation density increased by 21% at T_S = 60 °C and by 33% at T_S = 100 °C. Furthermore, the crystallite grain size significantly decreased. Fitting the nucleation density's temperature dependence to Equation 1 results in calculated crystal formation energy barriers of 35 ± 5 meV and 66 ± 3 meV for films of C_{60} out of ODCB and *p*-terphenyl out of CS_2, respectively. Section II in the Supporting Information details the nucleation density data analysis and the results of the $T_S > T_A$ experiments for both films are summarized in Fig. 4. The temperature dependent thin film growth experiment was repeated at lower temperatures (21 °C and 4 °C) in a different laboratory where otherwise the same experimental procedure was used. The nucleation density analysis revealed a similar *p*-terphenyl/CS_2 energy barrier of about 97 meV (Fig. S8). Although a limited temperature range is available for $T_S > T_A$ to keep T_S below the boiling point of the solvent, the results are in reasonable agreement with Arrhenius behavior that allows estimation of the nucleation energy barrier. However, the extracted E_i values are an order of magnitude smaller than those previously reported for organic small molecule crystalline thin films of vapor-deposited pentacene.[59] The discrepancy in the E_i values can possibly be attributed to solvation effects: solvent-substrate and solvent-molecule interactions heavily reduce the surface energy of growing, stable nuclei, decreasing the energy barrier to nucleation. The reduction of these surface effects in solution growth techniques like the PAC method could promote 2D growth by increasing molecule-substrate interactions relative to the molecule-molecule interaction energies in the crystal bulk.[61] 2D crystal growth of organic electronic materials has already been correlated to better device performance.[62,63] However, our SAM layer growth technique likely results in a more disordered monolayer compared to other SAM deposition techniques and promotes 3D growth.[59,62] AFM characterization of films grown using PAC indicates that the crystalline thin films are 3D (due to their 100-nm thicknesses) but have layered, 2D growth as shown in Fig. S9. Thus, the PAC method seems to encourage the 2D growth regime along long, needle-like crystallites at deposition temperatures much higher than those required by other deposition techniques despite the disordered underlying SAM.[61]

At higher temperatures, the growth enters a desorption-limited regime in which the molecules falling out of solution prefer to nucleate islands in more energetically favorable positions on the substrate rather than overcome the energy barrier to attach themselves to already formed islands. This regime is apparent in *p*-terphenyl films grown at $T_S > T_A$. The average length of the *p*-terphenyl crystalline needles decreased by almost 30% with increasing T_S as seen in Fig. 4c. Optimization of T_S is necessary to grow large, continuous crystallites suitable for device integration, although our results indicate that room temperature growths using PAC are the most favorable.

4. Conclusion

Using the PAC method, we have demonstrated the growth and orientation of millimeter-scale crystallites of organic small molecules (1) out of solution, (2) onto amorphous substrates, and (3) at ambient temperatures—all beneficial to promoting industrial organic semiconductor thin film growth. By varying the substrate temperature, pretreatment, and solvent, we optimized the solution growth of these materials and confirmed that our results follow trends predicted by known mechanisms of organic material heterogeneous nucleation and thin film growth. Our results yielded the longest thin film solution-processed *p*-terphenyl crystallites reported to date. The crystallinity of the films confirmed with GIWAXS, POM, and AFM data, coupled with their size and anisotropy make these solution-grown thin films candidates for integration into devices such as OFETs. Further work must be done to tune the solution growth to the specific material, but the optimizations of the PAC method presented are potentially transferrable to other commonly used solution-growth techniques. For instance, the crystal growth kinetics induced by the PAC method are similar to those induced by MGC methods. The PAC method grows thin films in a regime analogous to the transition regime of MGC methods. Thus, optimizations of crystal growth via surface pretreatment, solvent choice, and temperature could be directly applicable to MGC techniques such as blade coating, dip coating, and slot die coating.

Finally, the use of patterned PDMS along with optimization of the process parameters studied here could confer synergistic benefits, leading to even larger and intentionally-directed thin film structures. Overall, the material versatility and method transferability in these PAC optimizations opens the door to more accessible and scalable applications of crystalline organic small molecule thin films.

Conflicts of interest

There are no conflicts to declare.

Acknowledgements

This work was supported by the W. M. Keck Foundation under the "High Temperature Superconductivity in Organic Solids" project. This material is based upon work supported by the National Science Foundation Graduate Research Fellowship under Grant No. DGE 1650115 and the Materials Research Science and Engineering Center Grant DMR 1420736. We thank Dr. Nick Weadock for assistance with XRD data reduction.

References

1 V. Podzorov, E. Menard, A. Borissov, V. Kiryukhin, J. A. Rogers and M. E. Gershenson, *Physical Review Letters*, 2004, **93**, 086602.
2 J. H. Oh, H. W. Lee, S. Mannsfeld, R. M. Stoltenberg, E. Jung, Y. W. Jin, J. M. Kim, J. B. Yoo and Z. Bao, *Proceedings of the National Academy of Sciences of the United States of America*, 2009, **106**, 6065–6070.
3 A. S. Molinari, H. Alves, Z. Chen, A. Facchetti and A. F. Morpurgo, *Journal of the American Chemical Society*, 2009, **131**, 2462–2463.
4 K. Nakayama, Y. Hirose, J. Soeda, M. Yoshizumi, T. Uemura, M. Uno, W. Li, M. J. Kang, M. Yamagishi, Y. Okada, E. Miyazaki, Y. Nakazawa, A. Nakao, K. Takimiya and J. Takeya, *Advanced Materials*, 2011, **23**, 1626–1629.
5 H. F. Haneef, A. M. Zeidell and O. D. Jurchescu, *Journal of Materials Chemistry C*, 2020, 8, 759–787.
6 G. Gryn'Ova, K. H. Lin and C. Corminboeuf, *Journal of the American Chemical Society*, 2018, 140, 16370–16386.
7 V. C. Sundar, J. Zaumseil, V. Podzorov, E. Menard, R. L. Willett, T. Someya, M. E. Gershenson and J. A. Rogers, *Science*, 2004, **303**, 1644–1646.
8 G. Giri, E. Verploegen, S. C. B. Mannsfeld, S. Atahan-Evrenk, D. H. Kim, S. Y. Lee, H. A. Becerril, A. Aspuru-Guzik, M. F. Toney and Z. Bao, *Nature*, 2011, **480**, 504–508.
9 C. W. Sele, B. K. Charlotte Kjellander, B. Niesen, M. J. Thornton, J. B. P. H. Van Der Putten, K. Myny, H. J. Wondergem, A. Moser, R. Resel, A. J. J. M. Van Breemen, N. Van Aerle, P. Heremans, J. E. Anthony and G. H. Gelinck, *Advanced Materials*, 2009, **21**, 4926–4931.
10 D. T. James, J. M. Frost, J. Wade, J. Nelson and J. S. Kim, *ACS Nano*, 2013, **7**, 7983–7991.
11 S. Chen, Z. Li, Y. Qiao and Y. Song, *Journal of Materials Chemistry C*, 2021, **9**, 1126–1149.
12 T. He, M. Stolte, C. Burschka, N. H. Hansen, T. Musiol, D. Kälblein, J. Pflaum, X. Tao, J. Brill and F. Würthner, *Nature Communications*, 2015, **6**, 1–9.
13 C. Zhang, X. Zhang, X. Zhang, X. Fan, J. Jie, J. C. Chang, C. S. Lee, W. Zhang and S. T. Lee, *Advanced Materials*, 2008, **20**, 1716–1720.
14 H. Li, B. C. K. Tee, J. J. Cha, Y. Cui, J. W. Chung, S. Y. Lee and Z. Bao, *Journal of the American Chemical Society*, 2012, **134**, 2760–2765.
15 Z. Wang, R. Bao, X. Zhang, X. Ou, C. Lee, J. C. Chang and X. Zhang, *Angewandte Chemie International Edition*, 2011, **50**, 2811–2815.
16 L. Jiang, Y. Fu, H. Li and W. Hu, *Journal of the American Chemical Society*, 2008, **130**, 3937–3941.
17 A. L. Briseno, S. C. B. Mannsfeld, X. Lu, Y. Xiong, S. A. Jenekhe, Z. Bao and Y. Xia, *Nano Letters*, 2007, **7**, 668–675.
18 J. Chen, M. Shao, K. Xiao, Z. He, D. Li, B. S. Lokitz, D. K. Hensley, S. M. Kilbey, J. E. Anthony, J. K. Keum, A. J. Rondinone, W. Y. Lee, S. Hong and Z. Bao, *Chemistry of Materials*, 2013, **25**, 4378–4386.
19 Z. He, N. Lopez, X. Chi and D. Li, *Organic Electronics*, 2015, **22**, 191–196.
20 S. Bi, Z. He, J. Chen and D. Li, *AIP Advances*, 2015, **5**, 077170.
21 X. J. Zhang, J. S. Jie, W. Deng, Q. X. Shang, J. C. Wang, H. Wang, X. F. Chen and X. H. Zhang, *Advanced Materials*, 2016, **28**, 2475–2503.
22 A. M. Hiszpanski, S. S. Lee, H. Wang, A. R. Woll, C. Nuckolls and Y. L. Loo, *ACS Nano*, 2013, **7**, 294–300.
23 P. S. Jo, A. Vailionis, Y. M. Park and A. Salleo, *Advanced Materials*, 2012, **24**, 3269–3274.
24 C. Luo, A. K. K. Kyaw, L. A. Perez, S. Patel, M. Wang, B. Grimm, G. C. Bazan, E. J. Kramer and A. J. Heeger, *Nano Letters*, 2014, **14**, 2764–2771.
25 D.-M. Smilgies, R. Li, G. Giri, K. W. Chou, Y. Diao, Z. Bao and A. Amassian, *physica status solidi (RRL) - Rapid Research Letters*, 2013, **7**, 177–179.
26 D. M. Delongchamp, R. J. Kline, Y. Jung, D. S. Germack, E. K. Lin, A. J. Moad, L. J. Richter, M. F. Toney, M. Heeney and I. Mcculloch, *ACS Nano*, 2009, **3**, 780–787.
27 X. Gu, L. Shaw, K. Gu, M. F. Toney and Z. Bao, *Nature Communications*, 2018, **9**, 534.
28 S. S. Lee, S. B. Tang, D. M. Smilgies, A. R. Woll, M. A. Loth, J. M. Mativetsky, J. E. Anthony and Y. L. Loo, *Advanced Materials*, 2012, **24**, 2692–2698.
29 W. S. Hu, Y. T. Tao, Y. J. Hsu, D. H. Wei and Y. S. Wu, *Langmuir*, 2005, **21**, 2260–2266.
30 W. H. Lee, D. H. Kim, Y. Jang, J. H. Cho, M. Hwang, Y. D. Park, Y. H. Kim, J. I. Han and K. Cho, *Applied Physics Letters*, 2007, **90**, 132106.
31 J. W. Lee, Y. S. Choi and W. H. Jo, *Organic Electronics*, 2012, **13**, 3060–3066.
32 S. Qu and H. Tian, *Chemical Communications*, 2012, **48**, 3039–3051.
33 M. Akita, I. Osaka and K. Takimiya, *Materials*, 2013, **6**, 1061–1071.
34 K. Wu, T. Wu, S. Chang, C. Hsu and C. Wang, *Advanced Materials*, 2015, **27**, 4371–4376.
35 K. Lee, J. Kim, K. Shin and Y. S. Kim, *Journal of Materials Chemistry*, 2012, **22**, 22763–22768.
36 M. Cavallini, P. Stoliar, J.-F. Moulin, M. Surin, P. Leclère, R. Lazzaroni, D. W. Breiby, J. W. Andreasen, M. M. Nielsen, P.

Sonar, A. C. Grimsdale, K. Müllen and F. Biscarini, *Nano Letters*, 2005, **5**, 2422–2425.
37 K. Kim, M. Jang, M. Lee, T. K. An, J. E. Anthony, S. H. Kim, H. Yang and C. E. Park, *J. Mater. Chem. C*, 2016, **4**, 6996–7003.
38 K. S. Park, B. Cho, J. Baek, J. K. Hwang, H. Lee and M. M. Sung, *Advanced Functional Materials*, 2013, **23**, 4776–4784.
39 H. Kwon, K. Kim, T. K. An, S. H. Kim and C. E. Park, *Journal of Industrial and Engineering Chemistry*, 2019, **75**, 187–193.
40 K. Kim, Y. Rho, Y. Kim, S. H. Kim, S. G. Hahm and C. E. Park, *Advanced Materials*, 2016, **28**, 3209–3215.
41 K. Y. Wu, C. T. Hsieh, L. H. Wang, C. H. Hsu, S. T. Chang, S. T. Lan, Y. F. Huang, Y. M. Chen and C. L. Wang, *Crystal Growth and Design*, 2016, **16**, 6160–6166.
42 V. A. Postnikov, N. I. Sorokina, O. A. Alekseeva, A. A. Kulishov, R. I. Sokolnikov, M. S. Lyasnikova, V. V. Grebenev, O. V. Borshchev, M. S. Skorotecky, N. M. Surin, E. A. Svidchenko, S. A. Ponomarenko and A. E. Voloshin, *Crystallography Reports*, 2018, **63**, 819–831.
43 R.-S. Wang, Y. Gao, Z.-B. Huang and X.-J. Chen, 2017, 1–19.
44 H. Li, X. Zhou, S. Parham, T. Nummy, J. Griffith, K. N. Gordon, E. L. Chronister and D. S. Dessau, *Physical Review B*, 2019, **100**, 064511.
45 M. Gholinejad and H. R. Shahsavari, *Inorganica Chimica Acta*, 2014, **421**, 433–438.
46 Z. X. Zhao, Z. L. Hu, S. C. Yu and Q. X. Liu, *New Journal of Chemistry*, 2018, **42**, 13329–13338.
47 S. Kotha, A. K. Ghosh and K. D. Deodhar, *Synthesis*, 2004, **2004**, 549–557.
48 K. Sanechika, T. Yamamoto and A. Yammoto, *Bulletin of the Chemical Society of Japan*, 1984, **57**, 752–755.
49 Q.-X. Liu, D.-X. Zhao, H. Wu, Z.-X. Zhao and S.-Z. Lv, *Applied Organometallic Chemistry*, 2018, **32**, e4429.
50 T. Xue, D. Zhao, T. Hao, X. Li, T. Wang and J. Nie, *New Journal of Chemistry*, 2019, **43**, 6737–6745.
51 M. Yao, B. M. Andersson, P. Stenmark, B. Sundqvist, B. Liu and T. Wågberg, *Carbon*, 2009, **47**, 1181–1188.
52 C. Park, H. J. Song and H. C. Choi, *Chemical Communications*, 2009, 4803–4805.
53 L. Miozzo, A. Yassar and G. Horowitz, *Journal of Materials Chemistry*, 2010, **20**, 2513–2538.
54 A. A. Virkar, S. Mannsfeld, Z. Bao and N. Stingelin, *Advanced Materials*, 2010, **22**, 3857–3875.
55 Y. Guo, N. Karasawa and W. Goddard, *Nature*, 1991, **351**, 464–467.
56 M. M. Olmstead, F. Jiang and A. L. Balch, *Chemical Communications*, 2000, 483–484.
57 S. Cui, Y. Liu, G. Li, Q. Han, C. Ge, L. Zhang, Q. Guo, X. Ye and X. Tao, *Crystal Growth and Design*, 2020, **20**, 783–792.
58 A. P. Rice, F. S. Tham and E. L. Chronister, *Journal of Chemical Crystallography*, 2013, **43**, 14–25.
59 A. A. Virkar, S. C. B. Mannsfeld and Z. Bao, *Journal of Materials Chemistry*, 2010, **20**, 2664–2671.
60 A. Winkler, *Surface Science*, 2016, **652**, 367–377.
61 S. Verlaak, S. Steudel, P. Heremans, P. Heremans, D. Janssen, D. Janssen and M. Deleuze, *Physical Review B - Condensed Matter and Materials Physics*, 2003, **68**, 195409.
62 Y. Ito, A. A. Virkar, S. Mannsfeld, H. O. Joon, M. Toney, J. Locklin and Z. Bao, *Journal of the American Chemical Society*, 2009, **131**, 9396–9404.
63 A. Virkar, S. Mannsfeld, J. H. Oh, M. F. Toney, Y. H. Tan, G. Liu, J. C. Scott, R. Miller and Z. Bao, *Advanced Functional Materials*, 2009, **19**, 1962–1970.

